

Hybrid quantum cycle generative adversarial network for small molecule generation

Matvei Anoshin, Asel Saginalieva, Christopher Mansell, Vishal Shete, Markus Pflictsch, and Alexey Melnikov
Terra Quantum AG, 9000 St. Gallen, Switzerland

The contemporary drug design process demands considerable time and resources to develop each new compound entering the market. Generating small molecules is a pivotal aspect of drug discovery, essential for developing innovative pharmaceuticals. Uniqueness, validity, diversity, drug-likeness, synthesizability, and solubility molecular pharmacokinetic properties, however, are yet to be maximized. This work introduces several new generative adversarial network models based on engineering integration of parametrized quantum circuits into known molecular generative adversarial networks. The introduced machine learning models incorporate a new multi-parameter reward function grounded in reinforcement learning principles. Through extensive experimentation on benchmark drug design datasets, QM9 and PC9, the introduced models are shown to outperform scores achieved previously. Most prominently, the new scores indicate an increase of up to 30% in the druglikeness quantitative estimation. The new hybrid quantum machine learning algorithms, as well as the achieved scores of pharmacokinetic properties, contribute to the development of fast and accurate drug discovery processes.

I. INTRODUCTION

In the current pharmaceutical landscape, the drug design process is a prolonged and costly endeavor. It typically spans up to 15 years [1] from target identification to clinical application, incurring expenses of approximately 1 billion for each new drug. Machine Learning has shown successful uses through the different stages of drug development, from the search for specific protein inhibitors [2] to the evaluation of pharmacokinetic properties and adverse effects.

Generative Adversarial Networks (GANs) [3] have gained prominence in molecular design. Their architecture is adept at generating a vast array of potential drug candidates from extensive molecular spaces, thereby facilitating more efficient preliminary screenings. GAN models, especially when compared to recurrent neural networks [4] and variational autoencoders [5], have demonstrated superiority in generating SMILES [6] representations of compounds. The use of graph representations of compounds, which are invariant to the permutations of atom orders, has allowed GANs, particularly the MolGAN [7], to become state-of-the-art approach in generative chemistry.

Quantum-enhanced GANs, with their inherent probabilistic nature, offer a moderate advantage over their classical counterparts by encompassing a broader and more diverse chemical space [8]. However, in the current Noisy Intermediate-Scale Quantum (NISQ) era, the feasibility of purely quantum algorithms is limited. Here, hybrid algorithms may find a reasonable equilibrium between the high expressivity of modern quantum simulators and the stability of classical approaches.

Utilization of hybrid quantum neural networks (HQNNs) represents a convergence of classical deep learning architectures with Quantum Machine Learning (QML) algorithms [9–12], specifically through Parametrized Quantum Circuits (PQCs) [13]. This hybrid ap-

proach harnesses the strengths of classical and quantum computing, introducing a system capable of efficiently processing large datasets compared to classical deep learning architectures alone [14, 15]. HQNNs have exhibited promising applications across various industrial domains, including healthcare [16–18], chemistry [19, 20], routing [21] and aerospace [22], also in image classification [23, 24]. While HQNNs have demonstrated efficacy in these fields, further research is essential to explore their potential in drug design fully and to refine algorithms for enhanced robustness and scalability.

This article introduces the Hybrid Quantum Cycle MolGAN for generating graph representations of small molecules. By incorporating a Cycle Component into the Hybrid Quantum MolGAN (HQ-MolGAN), where both the Generator and the Cycle Component are represented using an HQNN [25, 26], we have been able to stabilize the training process for molecular samples and improve key metrics. This includes increases of up to 30% in the Quantitative Estimate of Druglikeness (QED score) [27]. Such models, have shown quantum superiority over classical MolGAN in all three key metrics QED, Synthesis Accessibility score (SA) [28] and logP (characteristic of the hydrophilicity and lipophilicity of a drug) [29]), as well as an advantage over nearest competitors among quantum models.

This work contributes insights into the potential of QML for small molecule generation, emphasizing the benefits of hybrid quantum-classical approaches in drug design. The results underscore the significance of employing quantum-enhanced models to achieve improved performance across essential molecular optimization metrics.

II. RESULTS

In this study, we introduce several models for small molecule generation. Firstly, we present a refined clas-

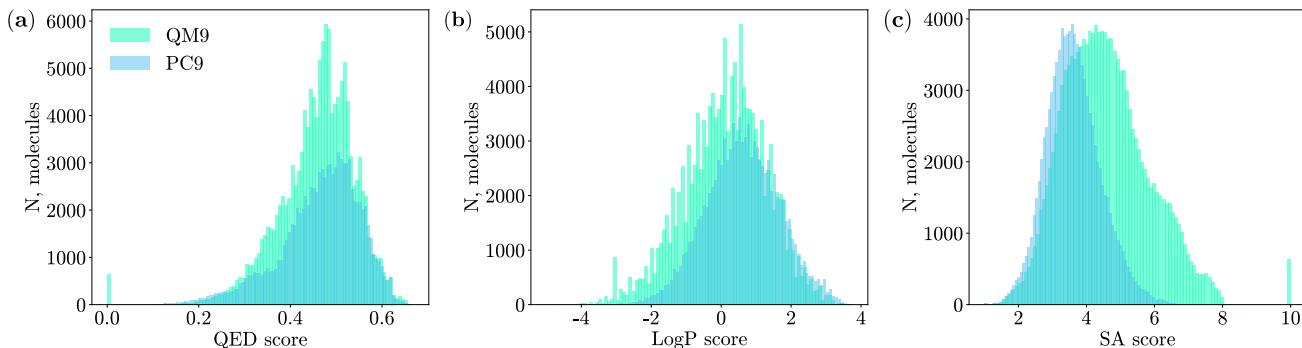


FIG. 1: Histograms of distribution of values of QED, SA and LogP scores in QM9 and PC9 datasets. The mean QED and LogP scores for molecules in the PC9 dataset are greater than those in QM9, while the mean score for SA is lower.

sical MolGAN with a halved parameter count, drawing inspiration from the state-of-the-art classical MolGAN architecture [7]. Secondly, in Sec. II we present an HQ-MolGAN, fusing classical and quantum computing approaches for enhanced capabilities. Notably, we propose the novel classical Cycle MolGAN, incorporating a multi-parameter reward function based on reinforcement learning principles, inspired by the state-of-the-art Cycle MolGAN [30]. Additionally, in Sec. II, we introduce the innovative Hybrid Quantum Cycle MolGAN (HQ-Cycle-MolGAN). Through rigorous experimentation on the QM9 and PC9 datasets, described in Sec. II, our results demonstrate that models trained on PC9 exhibit higher LogP scores than their QM9 counterparts. Furthermore, the hybrid quantum models showcase superior performance, achieving the highest QED, SA, and LogP metrics scores. Remarkably, our hybrid quantum model outperforms a similar QGAN-HG MR hybrid model from Ref. [8] and QuMolGAN from Ref. [31], emphasizing the efficacy of our proposed approaches in small molecule generation. We summarize our conclusions and outline future research directions in Sec. III.

Dataset

This study employed two datasets for model training: **QM9** and **PC9**. In this paper, two datasets were used for the training procedure. The QM9 dataset [32, 33], a well-established benchmark in small molecule drug design since 2012, comprises approximately 134,000 neutral molecules, each with no more than nine atoms (C, O, N, F) apart from hydrogen. Its comprehensive and diverse chemical space makes it particularly relevant for this field.

The second dataset, PC9, is a subset of the extensive PubChem database, containing around 99,000 molecules [34]. A notable distinction between QM9 and PC9 is that the latter includes not only neutral molecules but also those with a multiplicity greater than one. While PC9 was initially proposed as a replacement for the QM9 dataset, its practical usage alongside QM9 has demon-

strated benefits in generating a more diverse set of molecular structures.

Fig. 1 shows that the mean QED and LogP scores for molecules in the PC9 dataset are higher than those in QM9, while the mean score for Synthesis Accessibility (SA) is lower. Theoretically, this suggests that models trained on the PC9 dataset might be inclined to generate samples with higher values in these two key metrics than similar models trained on QM9. However, as detailed in Sec. II, this is not always the case.

It is important to note that during training, normalized values of logP, NP, and SA scores were evaluated and optimized.

HQ-MolGAN

In this section we introduce the HQ-MolGAN, which is based on classical MolGAN architecture [7]. As depicted in Fig.2 (a), green rectangular, the architecture of HQ-MolGAN is comprised of three primary components: the Generator (G), the Discriminator (D), and the Reward component (R). This model operates on the principles of the Wasserstein Generative Adversarial Network [35], wherein the Generator endeavors to synthesize molecular graph representations indistinguishable from authentic ones, thereby “deceiving” the Discriminator. The training regimen of HQ-MolGAN encapsulates a min-max optimization game, wherein the Generator and Discriminator engage in a continuous adaptive process to refine the generative quality of molecular representations:

$$\min_G \max_{D \in \mathcal{D}} \mathbb{E}_{\mathbf{y} \sim P_{\text{data}}} [D(\mathbf{y})] - \mathbb{E}_{\mathbf{z} \sim P_z} [D(G(\mathbf{z}))] - \underbrace{\lambda \mathbb{E}_{\hat{\mathbf{y}} \sim P_{\hat{\mathbf{y}}}} \left[\left(\|\nabla_{\hat{\mathbf{y}}} D(\hat{\mathbf{y}})\|_2 - 1 \right)^2 \right]}_{\text{gradient penalty}}.$$

The Reward Component in our HQ-MolGAN architecture functions as a sophisticated Reinforcement Learning objective, tasked with evaluating the Generator’s output based on several chemical property metrics. This

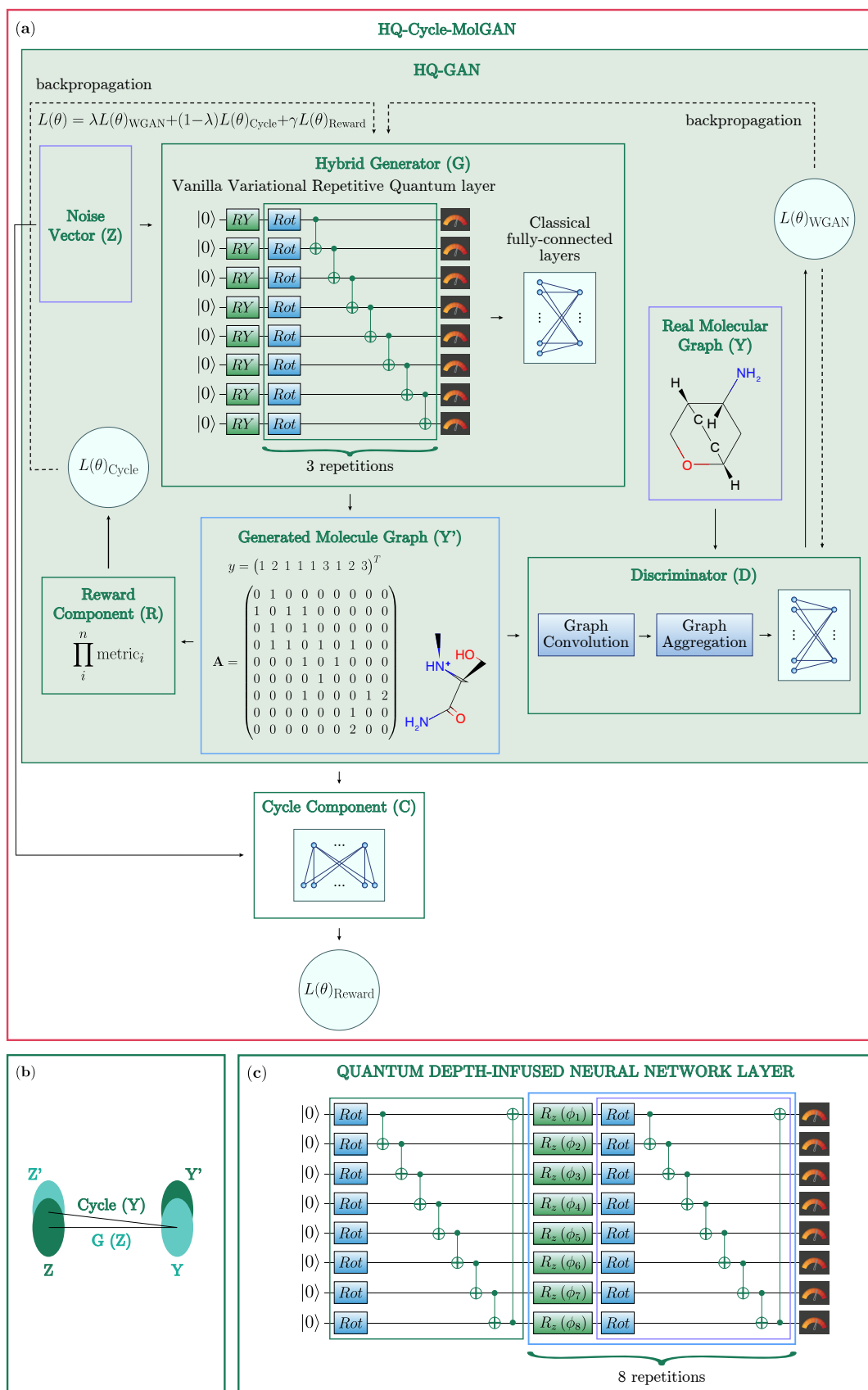


FIG. 2: **(a)** Structure of HQ-Cycle-MolGAN: Generator (G), Discriminator (D), Cycle Component (C). Highlighted with green part of HQ-Cycle-MolGAN is same for HQ-MolGAN. **(b)** Illustration of work of Cycle Components Let's suppose Z is a space of normally distributed noise vectors, Y -chemical space of datasets. Then Generator maps X to some chemical space Y' , and after Cycle Component restores vector $G(Z)$ back to noise. Then accuracy of these restorations is optimized. **(c)** Quantum Depth-Infused Neural Network Layer that was used as HQ-Cycle component.

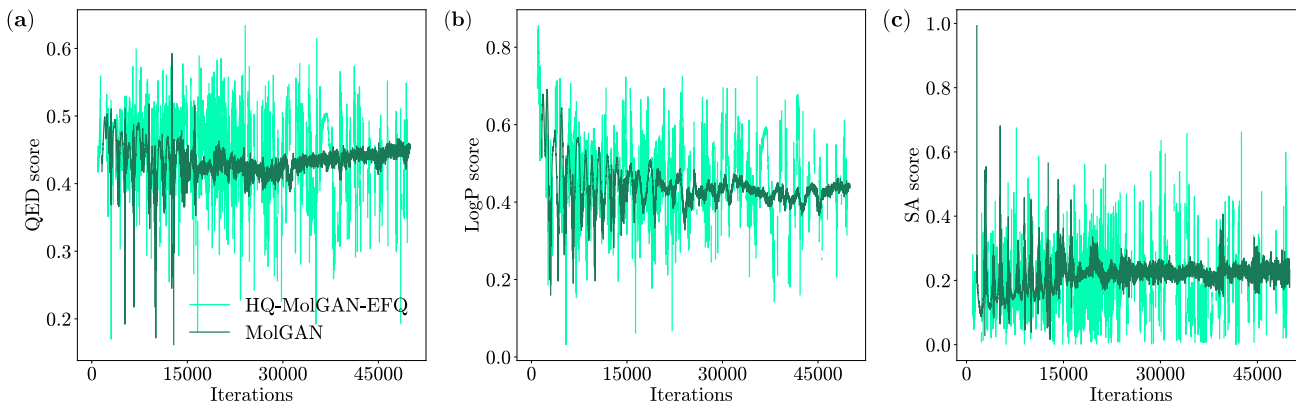


FIG. 3: Chart of (a) QED, (b) LogP, and (c) SA scores during training of classical MolGAN and Hybrid MolGAN. It can be seen that while MolGAN limits its scores to a narrow beam of values even after 50,000 iterations, when Hybrid MolGAN presents a wider range of compounds, covering greater scores of key metrics.

evaluation extends beyond the conventional metrics of Quantum Estimation of QED, LogP, and SA scores. It incorporates a comprehensive assessment of “validity”, quantified as the ratio of valid molecular samples to the total number of generated samples. Furthermore, it considers “novelty”, defined by the proportion of generated valid samples not present in the training dataset. Additionally, the Reward Component assesses “diversity”, a measure of the variance in the chemical structures of the generated molecules, and the “Natural Product likeness” (NP) score, as delineated by [36]. These multifaceted evaluation criteria enable a more nuanced and thorough assessment of the Generator’s performance, aligning the generated molecules more closely with desired chemical characteristics.

In the architecture of HQ-MolGAN, a pivotal role is played by the Variational Quantum Circuit (VQC), which is integrated as the initial layer in MolGAN’s generator. The VQC operates by encoding a noise vector into N qubits. Subsequent to the application of rotation and entanglement gates, the VQC outputs a probability distribution vector, denoted as $[p(0), \dots, p(2^N - 1)]$, where each element represents the probability of a corresponding quantum state. This vector, with a dimensionality of 2^N , undergoes a truncation process where only the first $2^{N-N_{\text{ancilla}}}$ elements are retained. The truncated vector is then fed into a classical fully-connected layers, which constitutes the remaining component of HQ-MolGAN’s generator.

In our experimental analysis, two distinct configurations of the VQC were evaluated: the Vanilla Variational Repetitive Quantum Layer (VVRQ) [37] and the Exponential Fourier Quantum Layer (EFQ) [38]. These configurations offer different approaches to quantum state transformation, thus providing a comparative understanding of their efficacy in the context of molecule generation.

The operational mechanism of the VVRQ layer within our HQ-MolGAN framework (Fig. 2 (a)) is as follows:

encoding the noise vector directly onto the qubits in a single step using angle embedding [39] (green rectangles in Fig. 2 (a)). Following this initialization, the VVRQ layer implements several variational layers which consist of a sequence of Rot (rotation) gates (blue rectangles in Fig. 2 (a))

$$\text{Rot}(\theta_1, \theta_2, \theta_3) = Ry(\theta_1) \cdot Rz(\theta_2) \cdot Ry(\theta_3)$$

$$Ry(\theta) = \begin{pmatrix} \cos(\frac{\theta}{2}) & -\sin(\frac{\theta}{2}) \\ \sin(\frac{\theta}{2}) & \cos(\frac{\theta}{2}) \end{pmatrix} \quad Rz(\theta) = \begin{pmatrix} \exp(-\frac{\theta}{2}) & 0 \\ 0 & \exp(\frac{\theta}{2}) \end{pmatrix}$$

and controlled NOT (CNOT) gates.

$$\text{CNOT} = \begin{pmatrix} 1 & 0 & 0 & 0 \\ 0 & 0 & 0 & 1 \\ 0 & 0 & 1 & 0 \\ 0 & 1 & 0 & 0 \end{pmatrix}$$

Originally this approach was proposed in [40] for image generation, but it can be applied to any generative task. The CNOT gates are applied between sequentially adjacent qubits, i.e., between qubit i and qubit $i + 1$, thereby facilitating quantum entanglement and information propagation across the qubit array.

This process is iteratively repeated for three variational layers, ensuring a thorough and complex manipulation of the quantum state. The final step in the VVRQ process involves measuring the probability distribution of the quantum states of the qubits. These measurements yield a probability vector that encapsulates the resultant quantum state post-entanglement and rotation, reflecting the encoded information from the initial noise vector.

In the EFQ layer the data encoding process is distinctly characterized by a dual-phase approach. Initially, the input data is encoded onto the qubits using angle embedding. This is followed by several variational layers, and

after this, a second encoding phase, wherein the amplitude of the rotational gates is systematically increased to double its initial value.

This dual encoding scheme, particularly with the amplified rotational amplitude in the second phase, is designed to enhance the expressive power of the quantum circuit [41]. By manipulating the amplitude of rotations in this manner, the EFQ layer is potentially able to induce a more diverse and complex quantum state space.

HQ-Cycle-MolGAN

The Cycle-MolGAN model introduces an innovative ‘‘Cycle component’’ (C) (Fig. 2 (b)) to the established MolGAN architecture. This component is ingeniously designed to reverse the molecule generation process. Specifically, it converts the generated molecular samples back into their originating noise vectors and assesses the accuracy of this reverse conversion. This approach, as proposed by [30], has been identified as particularly advantageous in the realm of molecular optimization tasks. It contributes significantly to the stability of the training performance and is instrumental in suppressing the training of the non-isomorphic generator compounds within the Hybrid-MolGAN framework, especially pertinent in the generation of small molecules.

Practically implemented, the Cycle component takes the form of a Multi-Layer Perceptron (MLP) model. This model effectively combines the adjacency matrix and the feature matrix of each generated molecular sample into a singular, unified tensor. Following this integration, the Cycle component proceeds to ‘‘mirror’’ the layers of the Generator, albeit in reverse order. This mirroring process is a critical step as it compresses the expanded dimensions of the combined tensor, specifically `batch_size` \times 405 from the adjacency matrix and `batch_size` \times 45 from the feature matrix, down to a more manageable size of `batch_size` \times 8. This reduction is pivotal for effectively re-encoding the complex molecular information back into the concise form of noise vectors.

In the development of the Hybrid Cycle component within the Cycle-MolGAN framework, we adhere to the classical design but with a crucial modification in the final layer. This layer is replaced by a Quantum Depth-Infused Neural Network Layer, as described in [42]. This quantum depth-infused layer undertakes the task of encoding a vector of size `batch_size` \times 64 into 8 qubits through a series of 8 repetitive encoding layers (blue rectangles in Fig. 2 (c)).

To optimize the performance of the Generator within this architecture, we employ a combined loss function, articulated as follows:

$$L(\theta) = \lambda \cdot L(\theta)_{\text{WGAN}} + (1 - \lambda) \cdot L(\theta)_{\text{Cycle}} + \gamma L(\theta)_{\text{Reward}}$$

$\gamma, \lambda \in [0, 1]$

This loss function integrates the Wasserstein GAN loss

($L(\theta)_{\text{WGAN}}$), the Cycle loss ($L(\theta)_{\text{Cycle}}$), and the Reward loss ($L(\theta)_{\text{Reward}}$). The coefficients γ and λ regulate the relative influence of each component in the overall loss calculation. In our experiments, we set λ to 0.5, thereby assigning equal importance to both cycles of transformation (from noise vector Z to generated sample Y' , and back from Y' to Z), as illustrated in Fig. 2 (b).

Training and Results

The models in this study were implemented using Python3, leveraging the PyTorch framework [43] and PennyLane [44] for quantum computations. For the evaluation of the chemical properties of the synthesized compounds, the RDKit library was employed. The computational experiments were conducted on high-performance GPU hardware, specifically the Tesla V100 and the RTX 3060.

For the classical MolGAN models, the generator’s architecture was scaled down by reducing the number of parameters in each layer by half, resulting in a total of 157,570 parameters in the Generator. The classical models, including both the standard MolGAN and Cycle-MolGAN, underwent a training regime of 200,000 iterations with a batch size of 10 samples. In contrast, the hybrid quantum models were subjected to a shorter training duration of 50,000 iterations. The validation set size was limited, containing either 100 samples when training on a single dataset or 250 samples in cases where multiple datasets were employed. In both EFQ and VVRQ models number of ancilla qubits is equal to 2.

The experimental investigation was conducted in three distinct stages:

- The First Stage (Sec. II A): This phase focused on evaluating the performance differences between the VVRQ and EFQ layers when integrated into the hybrid generator in HQ-MolGAN.
- The Second Stage (Sec. II B): The objective was to assess the impact of the classical Cycle Component on the performance of MolGAN and HQ-MolGAN.
- The Third Stage (Sec. II C): This stage involved an analysis of the Hybrid-Cycle Component, including a comparative study against the classical Cycle Component.

These three stages are described in detail in the next three subsections.

A. HQ-MolGAN

The investigation into the efficacy of the Hybrid Generator within the MolGAN framework commences with a comparative analysis focusing on the chemical properties of the generated molecular samples. Specifically,

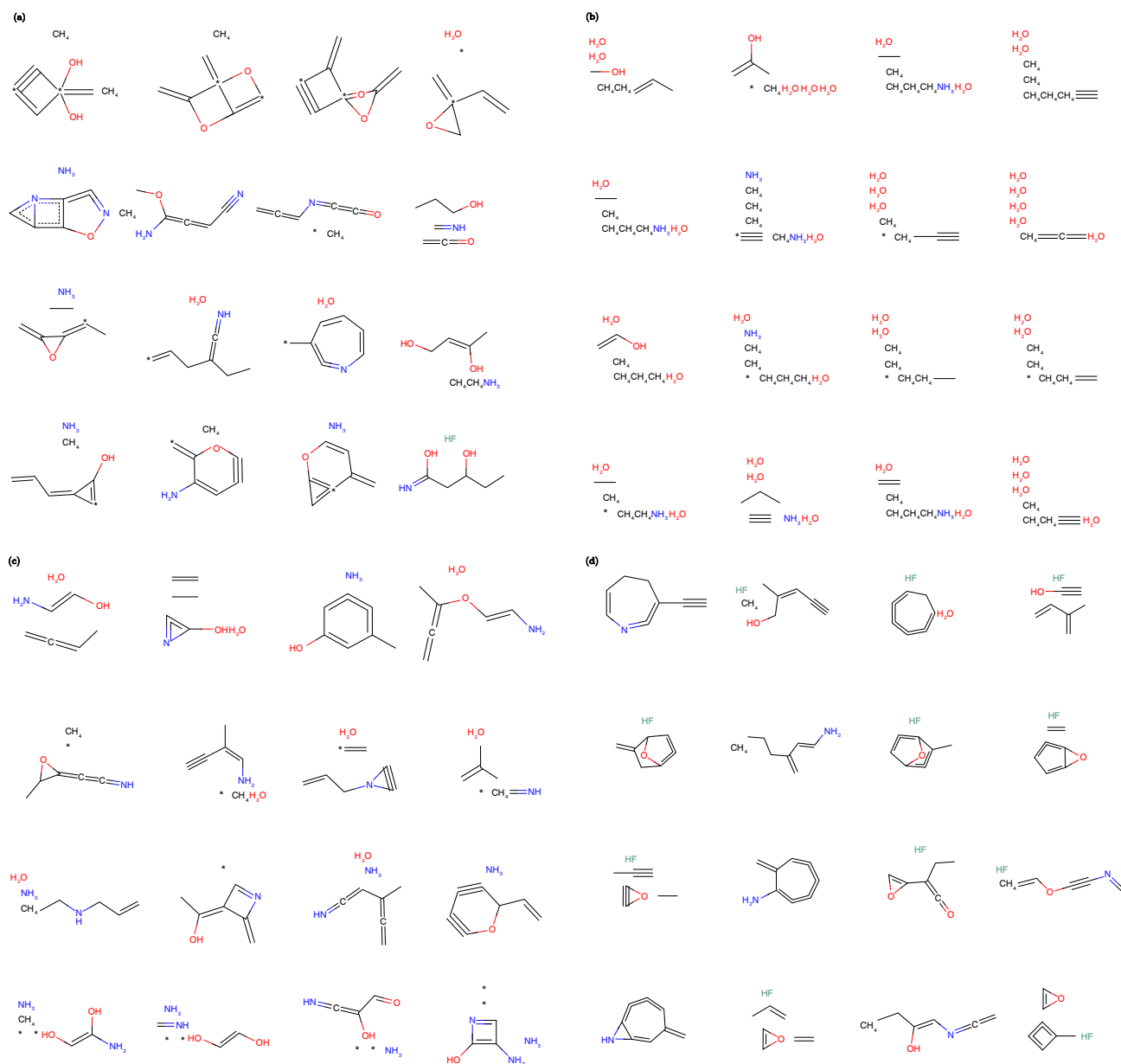


FIG. 4: (a) Samples generated by HQ-MolGAN-VVRQ trained on QM9. (b) “Highly entropy state”: HQ-MolGAN-VVRQ generated inappropriate samples and RDKit rewarded them with average metric of $\text{LogP} \propto 0.9$. (c) Samples generated by HQ-Cycle-MolGAN-VVRQ trained on Both datasets. (d) Samples generated by MolGAN with HQ-Cycle trained on Both datasets.

this analysis evaluates the logP and the QED scores. By contrasting the logP and QED scores yielded by the molecules generated from each model, we aim to quantify and elucidate the impact of the Hybrid Generator’s integration on the model’s performance in generating chemically viable and optimally structured molecules.

Fig. 3 illustrates a notable distinction in the behavior of the classical MolGAN and the HQ-MolGAN in terms of their generated molecular score distributions. The classical MolGAN model demonstrates a tendency to produce scores that converge towards a relatively nar-

row range. In contrast, the molecular samples generated by HQ-MolGAN exhibit an oscillatory behavior in their score values. This variability in the HQ-MolGAN’s scores can significantly influence the model’s training dynamics, particularly due to the Reward component which calculates the product of these metric values.

A potential explanation for the discontinuous score trends observed in the HQ-MolGAN could be attributed to its limited validation set size.

Nevertheless, the HQ-MolGAN capable to generate molecular samples with competitive scores in terms of

Drug-likeness, Synthesizability, and Solubility, as depicted in Fig. 4(a). As shown in Table I, the HQ-MolGAN-VVRQ model trained on the QM9 dataset achieves a LogP score of 0.84, the HQ-MolGAN-EFQ model trained on the PC9 dataset results in a QED score of 0.62, and the HQ-MolGAN-EFQ model trained on both datasets attains an SA score of 0.84.

The HQ-MolGAN-VVRQ model exhibits a propensity for generating samples with higher SA scores. In contrast, the HQ-MolGAN-EFQ model demonstrates superior performance in achieving greater QED and LogP scores.

Furthermore, a dataset-dependent variance in performance is observed. Models trained on the PC9 dataset consistently reach higher LogP scores compared to those trained on the QM9 dataset. This trend aligns with the inherent distribution of scores within these datasets, as illustrated in Fig. 1. However, such a correlation does not extend to the QED scores, where no discernible pattern is evident based on the choice of training dataset.

These findings underscore the nuanced impact of model configuration and training dataset on the performance of HQ-MolGAN in generating molecular samples with desired chemical properties. They highlight the need for careful consideration of both the model architecture and the dataset characteristics in optimizing the performance of molecule generation models.

During our experiments, a notable limitation of the Hybrid models was observed, characterized by a tendency of the generator to gravitate towards a "high entropy state". This phenomenon is illustrated in Fig. 4(b)). In this state, the generator predominantly produces molecular structures that are either bare, unbound atoms or a collection of disconnected small molecules. Intriguingly, despite their simplistic and fragmented nature, these structures are often assigned high scores in terms of LogP and SA by the RDKit library within the Reward component. This paradoxical scoring poses a challenge to the model’s reliability in generating chemically meaningful and complex molecules.

This observation indicates a critical issue in the mapping process of the generator. Essentially, a variety of noise samples Z are being mapped to a limited and similar region in the chemical space Y' , resulting in repetitive and high-entropy molecular samples. Such a mapping significantly diminishes the expressivity of the Generator, constraining its ability to generate a diverse range of molecular structures.

To ensure that the models generate unique and varied molecular samples, it is imperative to establish a one-to-one correspondence between different noise vectors and distinct molecular structures. In other words, the model must possess isomorphic properties to map distinct noise vectors to chemically diverse molecular samples. To achieve this objective, the integration of a Cycle component is proposed. The Cycle component is designed to reinforce the isomorphic nature of the model by facilitating a more diverse and accurate mapping from noise

vectors to molecular samples and vice versa, thereby enhancing the model’s capability to generate a wider array of unique molecular structures.

B. HQ-Cycle-MolGAN

Prior to assessing the effect of the Cycle component on the training of HQ-MolGAN, it is essential to first examine its impact on the conventional MolGAN framework. As indicated in Fig. 5(a), the incorporation of the Cycle component into MolGAN (termed Cycle-MolGAN) results in a more stable training process compared to the ordinary MolGAN model. This stability significantly enhances the quality of the generated molecular samples, as reflected in their improved Diversity scores (Table I, II). Furthermore, the Cycle component contributes to the generation of more complex and "bounded" molecular structures, indicating a higher degree of chemical realism.

In the context of HQ-MolGAN, while the integration of the Cycle component does not markedly alter the Loss curve as depicted in Fig. 5(b), its influence is evident in the improved key metric scores of the final HQ-Cycle-MolGAN models. Whether trained on the PC9 dataset or on a combination of datasets, the HQ-Cycle-MolGAN demonstrates superior performance in key metrics, as shown in Table II. The stabilizing properties of the Cycle component aid the model in consistently generating "bounded" molecular samples. Notably, both the VVRQ and EFQ variants of HQ-MolGAN achieve significant scores in terms of LogP (**0.93** and **0.94**) and QED.

Additionally, an analysis of Tables I and II reveals that models equipped with the Cycle component are capable of producing a greater number of unique samples. This finding aligns with the intended objective of the Cycle component, which is to navigate through the "high entropy state" and enhance the diversity and uniqueness of the molecular samples generated by the model.

C. Hybrid-Quantum Cycle MolGAN

In the third and final stage of our experimental series, we focused on evaluating the impact of the Hybrid-Quantum Cycle Component on both the classical MolGAN and the HQ-MolGAN architectures.

Fig. 6 presents a comparative analysis of the Generator losses between MolGAN and HQ-MolGAN models with and without the Hybrid-Quantum Cycle Component. According to the data presented in Table III, the incorporation of the Hybrid-Quantum Cycle Component does not result in significant improvements in most of the desired metrics, except for a notable LogP score of 0.95 achieved by the HQ-Cycle-MolGAN-VVRQ model trained on both datasets.

This absence of a marked enhancement in performance metrics for models incorporating the HQ-Cycle compo-

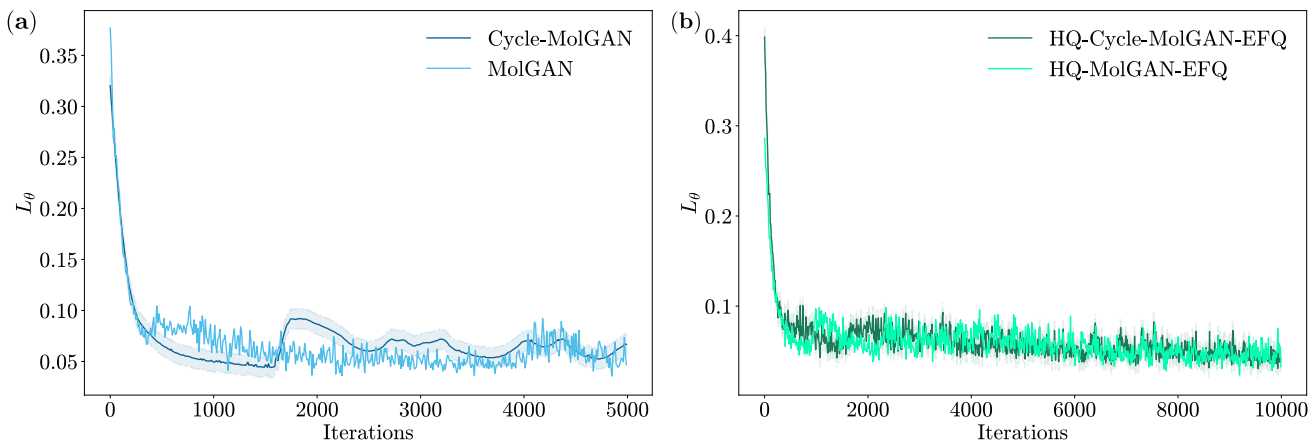


FIG. 5: Comparison of combined losses during training on the QM9 dataset. (a): Cycle-MolGAN versus MolGAN models, Cycle-MolGAN has a more stable training process compared to the MolGAN. (b): HQ-Cycle-MolGAN-EFQ versus Hybrid-MolGAN-EFQ, no significant impact of Cycle component on Loss curve observed.

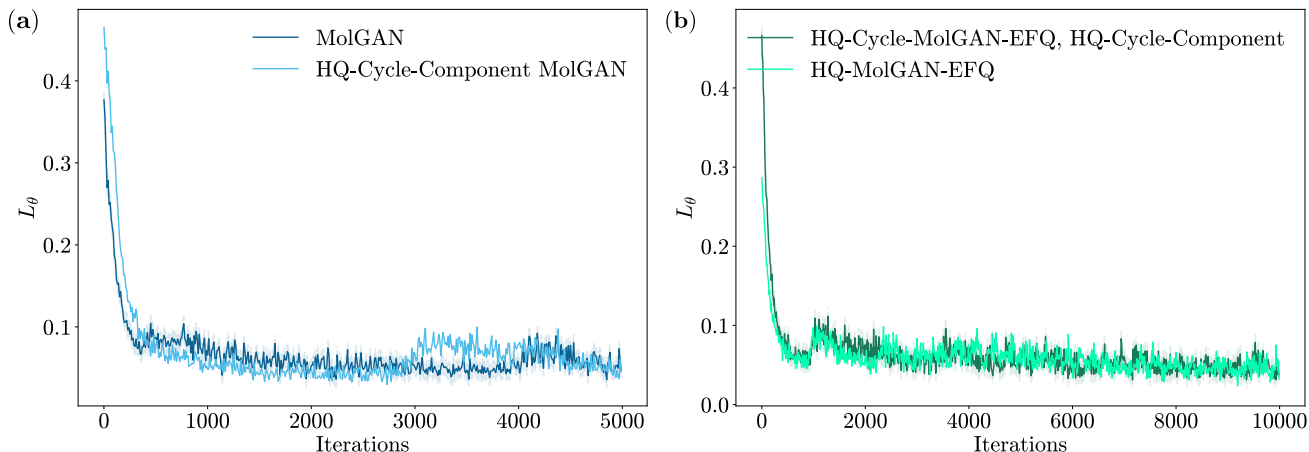


FIG. 6: (a) Graph of combined losses of MolGAN and HQ-Cycle Component MolGAN models trained on QM9 dataset. (b): Graph of combined losses of HQ-Cycle-MolGAN-EFQ and HQ-MolGAN-VVRQ models trained on QM9 dataset.

ment, as compared to their counterparts without it, could potentially be attributed to an insufficient number of training iterations. This hypothesis is supported by the observations from Fig. 6, where the training losses of MolGAN and MolGAN with the HQ-Cycle component exhibit minimal divergence, suggesting that extended training might be necessary for realizing the full potential of the HQ-Cycle Component.

Interestingly, the introduction of the Hybrid-Quantum Cycle Component appears to significantly elevate the “Unique” score of the models, surpassing even that achieved with the standard Cycle component. This outcome validates our initial hypothesis that a more precise generation of unique molecular samples is feasible, even with complex models like HQ-Cycle-MolGAN-EFQ or HQ-Cycle-MolGAN-VVRQ. This finding underscores the effectiveness of the HQ-Cycle Component in enhancing the diversity and uniqueness of the generated molecular structures.

III. DISCUSSION

In this article, we propose a novel approach leveraging QML for small molecule generation. Our chosen task of small molecule generation serves as a benchmark for the performance of hybrid quantum machine learning models.

To enhance the classical MolGAN, we introduce two solutions: the incorporation of VQCs as the initial layer of the generator and the utilization of a cycle component to restore the original data from the graph representation of the generated molecule.

Our empirical results substantiate the merit of diversifying training datasets, not limiting to the QM9 dataset alone but also incorporating the PC9 dataset or a combination of both. Notably, the HQ-MolGAN model, with their Generator’s layers scaled down by half and trained for a quarter fewer iterations, has outperformed the clas-

TABLE I: MolGAN and HQ-MolGAN

Model	Unique (%)	Valid (%)	Diversity	Druglikeliness	Synthesizability	Solubility
MolGAN (QM9)	63.0	1.1	0.98	0.47	0.64	0.52
MolGAN (PC9)	39.9	14.6	0.96	0.51	0.38	0.80
MolGAN (Both Datasets)	46.2	3.7	0.99	0.53	0.42	0.68
HQ-MolGAN-VVRQ (QM9)	71.1	14.3	0.97	0.53	0.84	0.61
HQ-MolGAN-VVRQ (PC9)	65.7	3.2	0.99	0.51	0.40	0.66
HQ-MolGAN-VVRQ (Both Datasets)	68.8	11.5	0.98	0.52	0.63	0.75
HQ-MolGAN-EFQ (QM9)	45.8	5.4	0.99	0.50	0.37	0.79
HQ-MolGAN-EFQ (PC9)	53.8	3.9	0.97	0.62	0.39	0.75
HQ-MolGAN-EFQ (Both Datasets)	39.4	12.9	0.97	0.53	0.49	0.84
QGAN-HG MR [8]	54.0	44.0	1.00	0.51	0.11	0.49
P2-QGAN-HG MR [8]	41.0	52.0	1.00	0.49	0.12	0.62
QuMolGAN [31]	5.4	42.94	1.00	0.57	0.76	0.44

TABLE II: MolGAN and HQ-MolGAN with classic Cycle component

Model	Unique (%)	Valid (%)	Diversity	Druglikeliness	Synthesizability	Solubility
Cycle-MolGAN (QM9)	86.3	0.7	1.00	0.47	0.37	0.46
Cycle-MolGAN (PC9)	67.8	3.2	0.98	0.48	0.27	0.52
Cycle-MolGAN (Both Datasets)	68.4	4.2	0.95	0.52	0.48	0.69
HQ-Cycle-MolGAN-VVRQ (QM9)	64.2	4.3	0.97	0.54	0.38	0.92
HQ-Cycle-MolGAN-VVRQ (PC9)	73.8	14.5	0.99	0.51	0.50	0.93
HQ-Cycle-MolGAN-VVRQ (Both Datasets)	86.7	6.8	0.98	0.58	0.48	0.75
HQ-Cycle-MolGAN-EFQ (QM9)	66.9	5.8	0.98	0.55	0.33	0.69
HQ-Cycle-MolGAN-EFQ (PC9)	81.2	22.1	0.96	0.54	0.40	0.94
HQ-Cycle-MolGAN-EFQ (Both Datasets)	64.1	7.5	0.98	0.53	0.35	0.66

TABLE III: MolGAN and HQ-MolGAN with Hybrid-Quantum Cycle component

Model	Unique (%)	Valid (%)	Diversity	Druglikeliness	Synthesizability	Solubility
Cycle-MolGAN (QM9)	92.4	2.7	0.99	0.47	0.35	0.64
Cycle-MolGAN (PC9)	93.2	5.1	0.97	0.46	0.28	0.65
Cycle-MolGAN (Both Datasets)	93.9	6.52	0.99	0.49	0.25	0.78
HQ-Cycle-MolGAN-VVRQ (QM9)	60.4	8.7	0.94	0.53	0.38	0.61
HQ-Cycle-MolGAN-VVRQ (PC9)	67.8	9.1	0.94	0.53	0.50	0.93
HQ-Cycle-MolGAN-VVRQ (Both Datasets)	65.5	15.0	0.98	0.51	0.35	0.95
HQ-Cycle-MolGAN-EFQ (QM9)	76.8	4.1	0.98	0.51	0.42	0.63
HQ-Cycle-MolGAN-EFQ (PC9)	88.8	11.0	0.98	0.50	0.35	0.69
HQ-Cycle-MolGAN-EFQ (Both Datasets)	74.7	9.3	0.96	0.52	0.49	0.73

sical MolGAN model [7] and its hybrid quantum analogues [8, 31] across key chemical metrics: QED, logP, SA and uniqueness.

The introduction of the HQ-Cycle-MolGAN, and especially its variant with the HQ-Cycle component, marks a significant advancement in the training of hybrid quantum models. These models not only enhance the desired uniqueness score but also effectively mitigate the occurrence of the ‘‘high entropy state’’, a notable challenge in molecular generation tasks. Consequently, these models hold substantial promise for applications in the domain of small drug compound design, both for commercial and scientific purposes within the pharmacology.

This work contributes insights into the potential of QML for small molecule generation, emphasizing the benefits of hybrid quantum-classical approaches in drug design. The results underscore the significance of employing quantum-enhanced models to achieve improved performance across essential molecular optimization met-

rics.

Looking ahead, we see a potential for hybrid quantum machine learning models to further advance the field of molecule generation using hybrid quantum models. We plan to delve deeper into refining the model architecture, particularly focusing on optimizing the balance between the quantum and classical components. This involves experimenting with different configurations and parameters to enhance the overall efficiency and accuracy of the models. Another critical avenue we intend to pursue is the expansion of our training datasets. By incorporating a broader range of chemical compounds and molecular structures, we aim to increase the diversity and representativeness of our models. This expansion is expected to improve the models’ generalization capabilities and their applicability. Through these focused research efforts, we aspire to contribute significantly to the advancement of hybrid quantum computing in drug discovery, ultimately aiding in the development of more effective and innova-

tive therapeutic solutions.

-
- [1] James P Hughes, Stephen Rees, S Barrett Kalindjian, and Karen L Philpott. Principles of early drug discovery. *British journal of pharmacology*, 162(6):1239–1249, 2011.
- [2] Feiqi Wang, Yun-Ti Chen, Jinn-Moon Yang, and Tatsuya Akutsu. A novel graph convolutional neural network for predicting interaction sites on protein kinase inhibitors in phosphorylation. *Scientific reports*, 12(1):229, 2022.
- [3] Ian J. Goodfellow, Jean Pouget-Abadie, Mehdi Mirza, Bing Xu, David Warde-Farley, Sherjil Ozair, et al. Generative Adversarial Networks. *arXiv preprint arXiv:1406.2661*, 2014.
- [4] Robin M. Schmidt. Recurrent Neural Networks (RNNs): A gentle Introduction and Overview. *arXiv preprint arXiv:1912.05911*, 2019.
- [5] Diederik P. Kingma and Max Welling. An introduction to variational autoencoders. *Foundations and Trends® in Machine Learning*, 12(4):307–392, 2019.
- [6] David Weininger. Smiles, a chemical language and information system. 1. introduction to methodology and encoding rules. *Journal of Chemical Information and Computer Sciences*, 28(1):31–36, 1988.
- [7] Nicola De Cao and Thomas Kipf. MolGAN: An implicit generative model for small molecular graphs. *arXiv preprint arXiv:1805.11973*, 2022.
- [8] Junde Li, Rasit O. Topaloglu, and Swaroop Ghosh. Quantum generative models for small molecule drug discovery. *IEEE Transactions on Quantum Engineering*, 2:1–8, 2021.
- [9] Sofiene Jerbi, Lukas J Fiderer, Hendrik Poulsen Nautrup, Jonas M Kübler, Hans J Briegel, and Vedran Dunjko. Quantum machine learning beyond kernel methods. *Nature Communications*, 14(1):517, 2023.
- [10] Adrián Pérez-Salinas, Radoica Draškić, Jordi Tura, and Vedran Dunjko. Reduce-and-chop: Shallow circuits for deeper problems. *arXiv preprint arXiv:2212.11862*, 2022.
- [11] Simon C Marshall, Casper Gyurik, and Vedran Dunjko. High dimensional quantum learning with small quantum computers. *arXiv preprint arXiv:2203.13739*, 2022.
- [12] Mo Kordzanganeh, Daria Kosichkina, and Alexey Melnikov. Parallel hybrid networks: an interplay between quantum and classical neural networks. *Intelligent Computing*, 2:0028, 2023.
- [13] Arsenii Senokosov, Alexander Sedykh, Asel Saginalieva, and Alexey Melnikov. Quantum machine learning for image classification. *arXiv preprint arXiv:2304.09224*, 2023.
- [14] YaoChong Li, Ri-Gui Zhou, RuQing Xu, Jia Luo, and WenWen Hu. A quantum deep convolutional neural network for image recognition. *Quantum Science and Technology*, 5(4):044003, 2020.
- [15] Kosuke Mitarai, Makoto Negoro, Masahiro Kitagawa, and Keisuke Fujii. Quantum Circuit Learning. *Physical Review A*, 98(3):032309, 2018.
- [16] Essam H Houssein, Zainab Abohashima, Mohamed Elhoseny, and Waleed M Mohamed. Hybrid quantum-classical convolutional neural network model for COVID-19 prediction using chest X-ray images. *Journal of Computational Design and Engineering*, 9(2):343–363, 2022.
- [17] Luca Lusnig, Asel Saginalieva, Mikhail Surmach, Tatjana Protasevich, Ovidiu Michiu, Joseph McLoughlin, et al. Hybrid quantum image classification and federated learning for hepatic steatosis diagnosis. *arXiv preprint arXiv:2311.02402*, 2023.
- [18] Prateek Jain and Srinjoy Ganguly. Hybrid quantum generative adversarial networks for molecular simulation and drug discovery. *arXiv preprint arXiv:2212.07826*, 2022.
- [19] Alexandr Sedykh, Maninadh Podapaka, Asel Saginalieva, Nikita Smertyak, Karan Pinto, Markus Pflitsch, et al. Quantum physics-informed neural networks for simulating computational fluid dynamics in complex shapes. *arXiv preprint arXiv:2304.11247*, 2023.
- [20] Andrii Kurkin, Jonas Hegemann, Mo Kordzanganeh, and Alexey Melnikov. Forecasting the steam mass flow in a powerplant using the parallel hybrid network. *arXiv preprint arXiv:2307.09483*, 2023.
- [21] Nathan Haboury, Mo Kordzanganeh, Sebastian Schmitt, Ayush Joshi, Igor Tokarev, Lukas Abdallah, et al. A supervised hybrid quantum machine learning solution to the emergency escape routing problem. *arXiv preprint arXiv:2307.15682*, 2023.
- [22] Serge Rainjonneau, Igor Tokarev, Sergei Iudin, Saaketh Rayaprolu, Karan Pinto, Daria Lemtiuzhnikova, et al. Quantum algorithms applied to satellite mission planning for Earth observation. *IEEE Journal of Selected Topics in Applied Earth Observations and Remote Sensing*, 16:7062–7075, 2023.
- [23] Asel Saginalieva, Andrii Kurkin, Artem Melnikov, Daniil Kuhmistrov, et al. Hybrid quantum ResNet for car classification and its hyperparameter optimization. *Quantum Machine Intelligence*, 5(2):38, 2023.
- [24] Jonas Landman, Natansh Mathur, Yun Yvonna Li, Martin Strahm, Skander Kazdaghli, Anupam Prakash, et al. Quantum methods for neural networks and application to medical image classification. *Quantum*, 6:881, 2022.
- [25] Michael Perelshtein, Asel Saginalieva, Karan Pinto, Vishal Shete, et al. Practical application-specific advantage through hybrid quantum computing. *arXiv preprint arXiv:2205.04858*, 2022.
- [26] Alexey Melnikov, Mohammad Kordzanganeh, Alexander Alodjants, and Ray-Kuang Lee. Quantum machine learning: from physics to software engineering. *Advances in Physics: X*, 8(1):2165452, 2023.
- [27] G Richard Bickerton, Gaia V Paolini, Jérémy Besnard, Sorel Muresan, and Andrew L Hopkins. Quantifying the chemical beauty of drugs. *Nature chemistry*, 4(2):90–98, 2012.
- [28] Peter Ertl and Ansgar Schuffenhauer. Estimation of synthetic accessibility score of drug-like molecules based on molecular complexity and fragment contributions. *Journal of cheminformatics*, 1:1–11, 2009.
- [29] Albert Leo, Corwin Hansch, and David Elkins. Partition coefficients and their uses. *Chemical Reviews*, 71(6):525–616, 1971.
- [30] Łukasz Maziarka, Agnieszka Pocha, Jan Kaczmarczyk, Krzysztof Rataj, Tomasz Danel, and Michał Warchoł. Mol-cyclegan: A generative model for molecular opti-

- mization. *Journal of Cheminformatics*, 12(1), 2020.
- [31] Po-Yu Kao, Ya-Chu Yang, Wei-Yin Chiang, Jen-Yueh Hsiao, Yudong Cao, Alex Aliper, et al. Exploring the Advantages of Quantum Generative Adversarial Networks in Generative Chemistry. *Journal of Chemical Information and Modeling*, 63(11):3307–3318, 2023.
- [32] Raghunathan Ramakrishnan, Pavlo O Dral, Matthias Rupp, and O Anatole Von Lilienfeld. Quantum chemistry structures and properties of 134 kilo molecules. *Scientific data*, 1(1):1–7, 2014.
- [33] Lars Ruddigkeit, Ruud van Deursen, Lorenz C. Blum, and Jean-Louis Reymond. Enumeration of 166 billion organic small molecules in the chemical universe database gdb-17. *Journal of Chemical Information and Modeling*, 52(11):2864–2875, 2012.
- [34] Marta Glavatskikh, Jules Leguy, Gilles Hunault, Thomas Cauchy, and Benoit Da Mota. Dataset’s chemical diversity limits the generalizability of machine learning predictions. *Journal of Cheminformatics*, 11(1):69, 2019.
- [35] Martin Arjovsky, Soumith Chintala, and Léon Bottou. Wasserstein GAN. *arXiv preprint arXiv:1701.07875*, 2017.
- [36] Peter Ertl, Silvio Roggo, and Ansgar Schuffenhauer. Natural product-likeness score and its application for prioritization of compound libraries. *Journal of Chemical Information and Modeling*, 48(1):68–74, 2007.
- [37] Mohammad Kordzanganeh, Markus Buchberger, Basil Kyriacou, Maxim Povolotskii, Wilhelm Fischer, Andrii Kurkin, et al. Benchmarking simulated and physical quantum processing units using quantum and hybrid algorithms. *Advanced Quantum Technologies*, 6(8):2300043, 2023.
- [38] Mo Kordzanganeh, Pavel Sekatski, Leonid Fedichkin, and Alexey Melnikov. An exponentially-growing family of universal quantum circuits. *Machine Learning: Science and Technology*, 4(3):035036, 2023.
- [39] F. Bloch. Nuclear Induction. *Physical Review*, 70(7-8):460–474, 1946.
- [40] Shu Lok Tsang, Maxwell T. West, Sarah M. Erfani, and Muhammad Usman. Hybrid quantum–classical generative adversarial network for high-resolution image generation. *IEEE Transactions on Quantum Engineering*, 4:1–19, 2023.
- [41] Maria Schuld, Ryan Sweke, and Johannes Jakob Meyer. Effect of data encoding on the expressive power of variational quantum-machine-learning models. *Physical Review A*, 103(3), 2021.
- [42] Asel Sagingalieva, Mohammad Kordzanganeh, Nurbolat Kenbayev, Daria Kosichkina, Tatiana Tomashuk, and Alexey Melnikov. Hybrid quantum neural network for drug response prediction. *Cancers*, 15(10):2705, 2023.
- [43] PyTorch — Machine Learning framework. <https://pytorch.org/>, 2022.
- [44] Ville Bergholm, Josh Izaac, Maria Schuld, Christian Gogolin, M Sohaib Alam, et al. PennyLane: Automatic differentiation of hybrid quantum-classical computations. *arXiv preprint arXiv:1811.04968*, 2018.